Applied Surface Science 529 (2020) 147156

Contents lists available at ScienceDirect

Applied Surface Science

journal homepage: www.elsevier.com/locate/apsusc

Full Length Article

Laser-induced regular nanostructure chains within microgrooves of Fe-based metallic glass

Zhen Zhao[a,b], Bo Zhao[c], Yuhao Lei[d], Jianjun Yang[a,*], Chunlei Guo[e]

[a] State Key Laboratory of Applied Optics, Changchun Institute of Optics, Fine Mechanics and Physics, Chinese Academy of Sciences, Changchun 130033, China
[b] Center of Materials Science and Optoelectronics Engineering, University of Chinese Academy of Sciences, Beijing 100049, China
[c] Department of Electronic Information and Physics, Changzhi University, Shanxi 046011, China
[d] Optoelectronics Research Centre, University of Southampton, Southampton SO17 1BJ, United Kingdom
[e] The Institute of Optics, University of Rochester, Rochester, NY 14627, USA

ARTICLE INFO

Keywords:
Laser materials processing
Subwavelength structures
Nanostructures
Surface plasmons
Ultrafast phenomena

ABSTRACT

Femtosecond laser-induced surface structures have been extensively investigated over decades, however, their formation is not well controlled especially for the practical use in the photonic field. We here report the highly regular nanostructure formation within the grooves of the Fe-based metallic glass, upon irradiation of two temporally delayed femtosecond laser beams. For the case of micrometer-sized groove, multiple chains of spindle-like nanostructures are developed, with the spatial periods of 667 nm and 180 nm for the chain and spindle distributions, respectively. Their arrangement properties can be modulated by varying laser parameters. On the other hand, for the case of submicrometer-sized groove, there is only one chain of spindle-like nanostructures formed inside with the improved regular appearance. Two physical effects, including the plasmonic field generation from the groove edges and the surface magnon polariton excitation within the groove, are considered responsible for the phenomena, which consequently result in the spatial interlocking of two types of ripples. The theoretical analyses match well the experimental observations.

1. Introduction

Micro or nano-structuring of materials has opened up new possibilities in both fundamental research and applications [1,2], because it can effectively manipulate the material properties. Even though there are several fabrication technologies based on either top-down or bottom-up method, they are facing some major problems, such as the high costs, the low throughput and the lack of reproducibility [3–5]. Over recent years of the study, the femtosecond laser has been identified as a versatile tool for drilling, patterning, and synthesizing various types of micro- and nanostructures [6–9]. In particular, it is found that the ripple-like surface structures at subwavelength scales can be generated on materials upon femtosecond laser irradiation with the energy fluences near the ablation threshold [10,11], which inspires the great enthusiasm of high-speed large-area fabrication of nanostructures without masks.

As for the physical origins of the ripple-like structures, interference between the incident laser and the excited surface plasmon polaritons (SPP) was mostly considered [12,13]. Because of undergoing self-assembly processes during multi-pulsed laser irradiation, such structure formation was often difficult to control externally. At the initial stage of femtosecond laser irradiation, SPP noise induced spontaneously by the surface roughness brings out the weak ripple formation, and its coupling with many subsequent laser pulses tends to enhance the contrast, so that the obtained structures usually present wavy and non-regular appearance even on the flat material surfaces, and they are not satisfactory for photonic device applications [14]. As an efficient scattering source, the groove geometry would like to change the laser-material interactions, which makes the physical scenario more complicated. On the other hand, a number of works have shown that magnetic materials can excite surface magnon polaritons (SMP) [15,16]. Under such circumstances, the transverse electric (TE) polarized surface waves can be generated by the incident light [17,18]. However, the corresponding formation of the surface structures has not yet been seen in the experiment.

In this paper, we report the controllable formation of the regular chains of spindle-like nanostructures within the microgrooves scratched on the Fe-based metallic glass surface, upon irradiation of two femtosecond laser beams at certain temporal delays. The measured periods of the chains and the spindle units are in subwavelength and deep-

* Corresponding author.
E-mail address: jjyang@ciomp.ac.cn (J. Yang).

https://doi.org/10.1016/j.apsusc.2020.147156
Received 8 March 2020; Received in revised form 29 June 2020; Accepted 1 July 2020
Available online 07 July 2020
0169-4332/

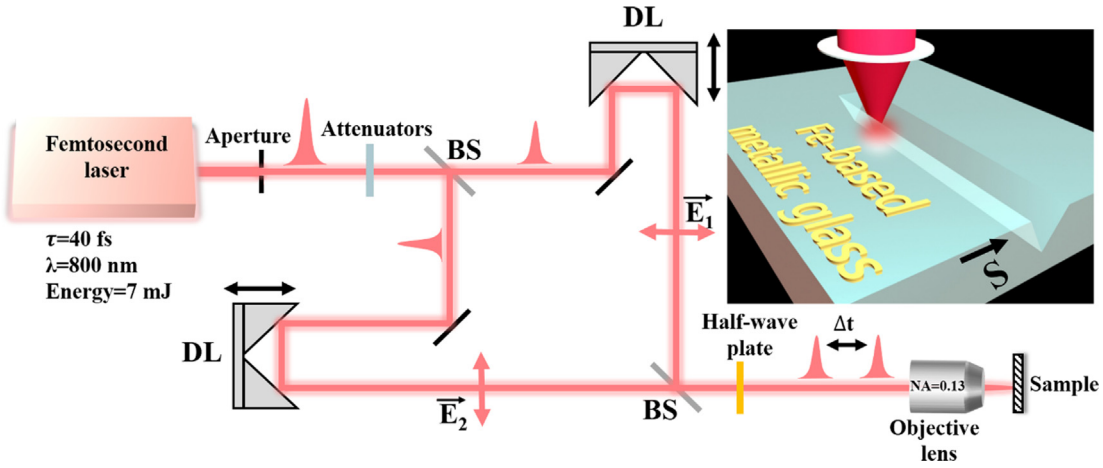

Fig. 1. Schematic diagram of the experimental setup for the formation of spindle-like nanostructure chains inside the grooves of Fe-based metallic glass, with irradiation of double temporally delayed femtosecond laser beams. τ: pulse width; λ: central wavelength of the laser pulse; BS: beam splitter; DL: delay line; Δt: delay time; NA: numerical aperture; E_1 and E_2: electric field (or the polarization direction) of two laser beams, S for the direction of the sample scanning.

subwavelength scales. The nanostructure size and orientation can be effectively manipulated with variable laser parameters. It is also found that the groove width can affect the formation of spindle-like nanostructures including the number of chains and the arrangement regularity. The underlying mechanisms are then discussed with considering the coherent SPP generation and excitation of SMP inside the grooves. Meanwhile, the chain of spindle-like nanostructures can be expected for manipulation of the light in subwavelength scale to produce the phenomena of optical trapping [19], surface enhanced Raman scattering [20], plasmon waveguides [21], and other potential applications in the fields of optoelectronic, solar energy, sensing, etc.

2. Experimental arrangement

The experimental setup is schematically shown in Fig. 1, where a commercial Ti: sapphire femtosecond laser amplifier system (Spectra Physics HP-Spitfire 50) was employed as the light source to deliver the laser pulses with a central wavelength of 800 nm at a repetition rate of 1 kHz. The measured pulse duration was 40 fs and the maximum pulse energy up to 7 mJ. The laser energy was controlled by neutral density attenuators. After being divided into two parts by a beam splitter, the output laser was guided into two optical arms with different optical lengths for the temporally delayed propagation (E_1, E_2). Afterwards, they were spatially aligned into collinear overlapping and focused by an objective lens (Nikon, 4×, N.A = 0.13) onto a sample at normal incidence. The two laser polarizations can be simultaneously changed by a half-wave plate. A hard aperture with a diameter of 3.2 mm was employed in the main optical path to acquire a homogeneous laser intensity distribution of the beam spot [22]. Of course, the single-beam femtosecond laser irradiation can also be obtained by blocking one of the optical arms.

In the experiment, a Fe-based metallic glass ($Fe_{85}Si_9B_6$) foil with 40 μm thickness was adopted as the sample material, by considering its superior physical and chemical properties such as soft magnetic properties, excellent corrosion and wear resistance [23–25]. On the sample surface there exist two mechanically scratched grooves, with the feature dimension at the micron and submicron scales, respectively. Their morphology characterizations by scanning electron microscopy (SEM, HITACHI, S-4800) and atomic force microscopy (AFM, BRUKER, Multimode 8) are shown in Fig. 2. From the cross-section measurement, we can find that the two grooves are V-shaped in geometry with the smooth sidewall surfaces. For one groove, the measured average opening width and depth approximate 3.80 ± 0.04 μm and 627 ± 8 nm, respectively; whereas for the other groove, the average opening width and depth are shrunk to 930 ± 65 nm and 90 ± 9 nm, respectively. The sample was mounted on a computer-controlled three-axis translation stage, and the line-scanning method was carried out under the fixed laser irradiation. To avoid the strong ablation damage, the sample was moved about 600 μm away from the focus along the opposite direction of the laser propagation, and the calculated focal beam spot on the sample surface is approximately 78 μm in the radius. The experiment was carried out in ambient air environment using a line-scribing method with at the scanning speed of 0.3 mm/s under the fixed irradiation of lasers, resulting in 520 pulses partially overlapped within one laser spot area. The laser fluence was calculated using a formula of $F = 2E_0/\pi w_z^2$, with E_0 being the pulse energy and w_z being the focused beam spot radius on the sample surface.

The near-field intensity distribution within the microgroove under the laser irradiation was simulated using the three-dimensional finite difference time domain (3D-FDTD) method (Lumerical FDTD solutions software package). The dimensions of the microgroove with the V-shape profile were set as a width of 3.8 μm and a depth of 600 nm. The simulation region is a cubic box with a dimension of 20 × 1 × 0.7 μm^3. The boundaries of the simulation region were truncated by perfectly matched layers, while the front and rear sides were set as periodic boundary conditions. The light source was a transverse magnetic (TM) polarized monochromatic plane wave with the wavelength of 800 nm, which illuminates the microgroove at normal incidence. The optical refractive index of the material is n = 3.06 + 3.95i at the wavelength of 800 nm, which was extracted from the measured data by an ellipsometer (Semilab, GES5-E). Given the influence of the surface roughness, the effective refractive index with the microgroove was modified as n = 1.65.

3. Experimental results and discussions

3.1. Formation of multiple nanostructure chains within the microgroove

Fig. 3 shows the surface morphology change inside the microgroove with irradiation of two femtosecond laser beams at the temporal delay of Δt = 6 ps, where two laser beams have the identical energy fluences of F = 21 mJ/cm^2, and the sample is scanned at the speed of v = 0.3 mm/s along the direction perpendicular to the groove orientation but parallel to the laser polarization. From the SEM image in Fig. 3a, we can surprisingly find there are five nanostructure chains formed within the microgroove, each of which is arranged in the direction parallel to the groove edges. Interestingly, the formation of such multiple nanostructure chains is seen continuously extended in the whole laser-exposed areas. The spacing between two neighboring chains was measured about 667 nm. A high-resolution image reveals

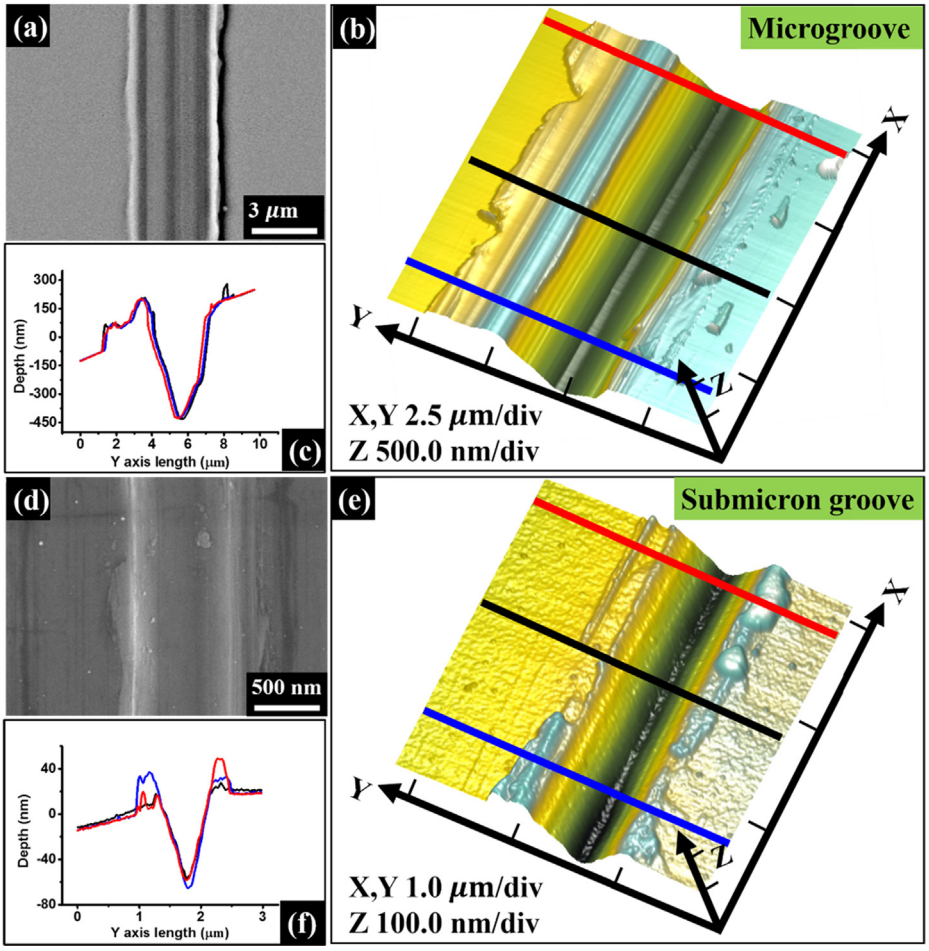

Fig. 2. Microscopic images of two grooves mechanically scratched on Fe-based metallic glass, associated with the feature sizes of micron (a)–(c) and submicron (d)–(f) scales. (c) and (f) indicate the measured cross section profiles (red, black, blue lines) at different positions for two grooves. (For interpretation of the references to colour in this figure legend, the reader is referred to the web version of this article.)

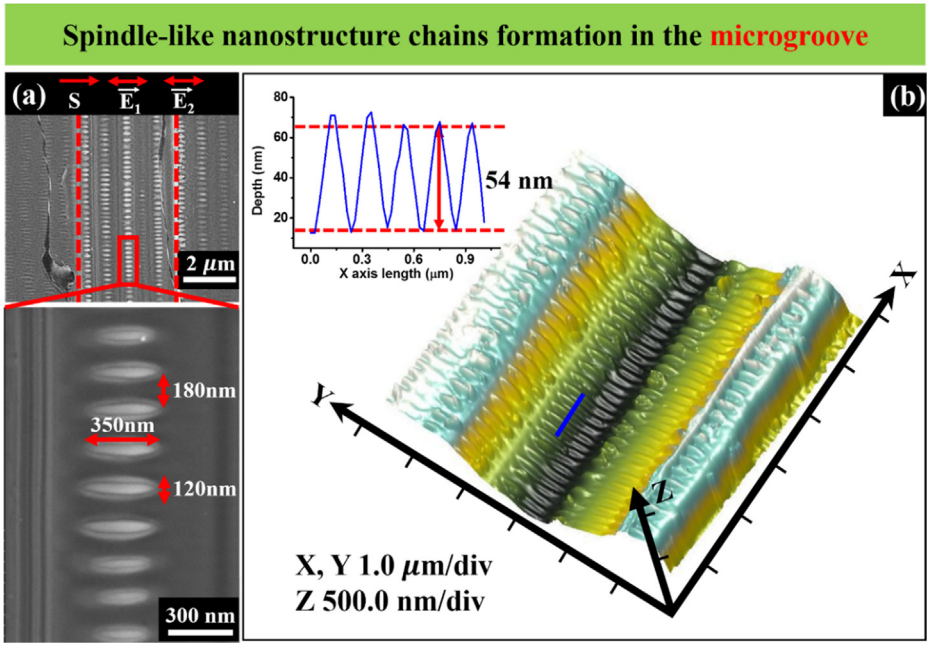

Fig. 3. Observed formation of the spindle-like nanostructure chains within the microgroove irradiated by two femtosecond laser beams at the time delay of $\Delta t = 6$ ps, where the incident total energy fluence is $F = 42$ mJ/cm^2 and the scanning speed is $v = 0.3$ mm/s. (a) SEM images of the multiple chains of spindle-like nanostructures. Here E_1 and E_2 represent directions of the laser polarization, and S for the sample scanning direction. The red dashed lines mark the edges of the microgroove. (b) Three-dimensional AFM measurements of the microgroove covered with spindle-like nanostructures, and the upper-left inset shows the measured cross section curve for a small portion of nanostructure formation (blue line) inside the groove. (For interpretation of the references to colour in this figure legend, the reader is referred to the web version of this article.)

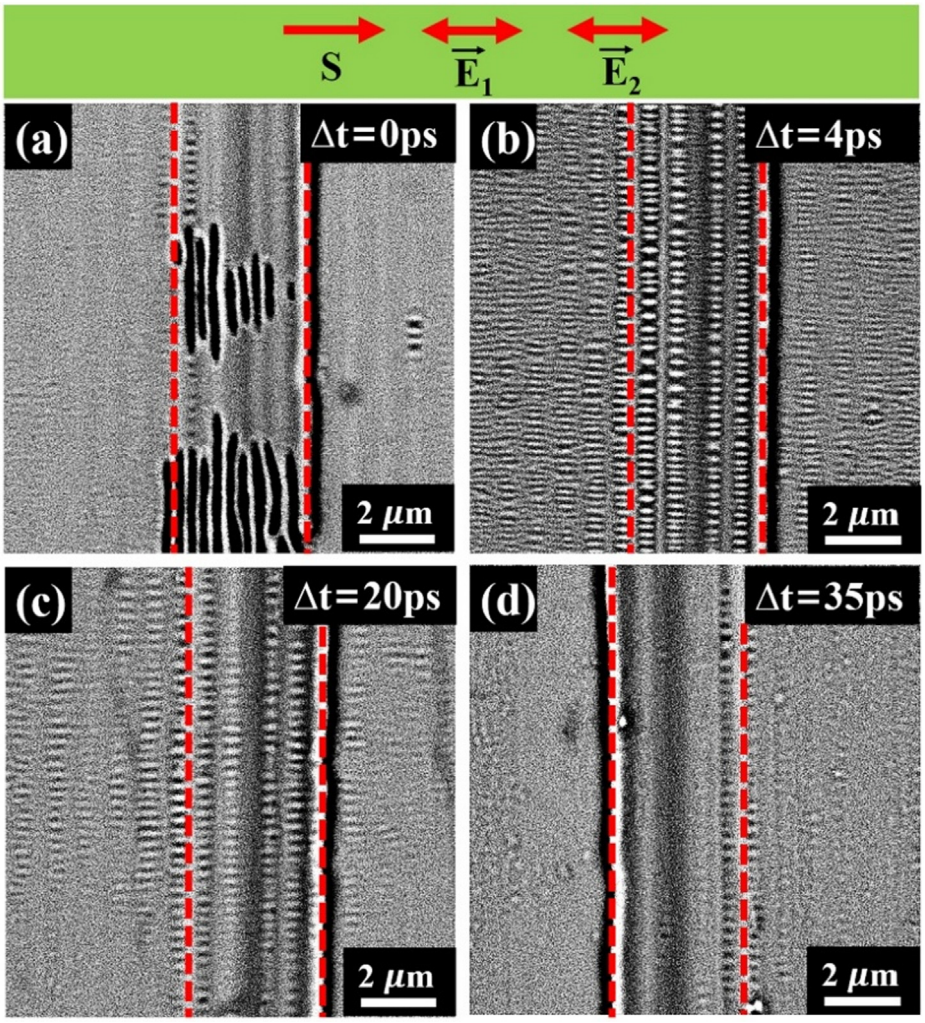

Fig. 4. Formation of spindle-like nanostructure chains inside the microgroove with varying time delay of two laser beams. (a) $\Delta t = 0$ ps, (b) $\Delta t = 4$ ps, (c) $\Delta t = 20$ ps and (d) $\Delta t = 35$ ps. The total incident laser energy fluence is $F = 42$ mJ/cm^2, and the scanning speed is $v = 0.3$ mm/s.

that each chain is constituted by the well-defined structure units with the spindle-like appearance. For each spindle unit, both major and minor lengths are about 120 nm and 350 nm, respectively. Meanwhile the spatial period of the spindle unit distribution was measured about $\Lambda = 180$ nm. These results suggest that the obtained structures can possess the dimension smaller than a quarter of the incident laser wavelength ($\lambda = 800$ nm). Moreover, from the three-dimensional (3D) measurement of AFM for the larger groove situation, as shown in Fig. 3b, it is also found that the formation of spindle nanostructure chains is located not only on the bottom but also on the sidewalls, which unavoidably increase surface roughness of the groove. The obtained cross section curve of the nanostructure distribution, as shown by the upper-left inset of Fig. 3b, demonstrates that the modulation height of the spindle units approximates 54 nm. During the experiment, when the incident laser fluence reduced down to about $F = 20$ mJ/cm^2, the formation of the spindle-like nanostructures can only be localized inside the microgroove, associated with degraded spatial regularity and the modulation depth.

3.2. Influence of the laser parameters on the structure formation

To comprehensively investigate the formation of spindle chains inside the microgroove, we began to vary the incident laser parameters in the experiment, such as the time delay between two lasers, the direction of laser polarization, and the pulse energy fluence. Fig. 4 shows the evolution of the surface morphology inside the microgroove with the time delay between double laser beams, while other laser parameters are kept the same with Fig. 3. For example, at $\Delta t = 0$ ps, *i.e.*, when two femtosecond laser beams are incident simultaneously, it was found that some areas of the groove surface were seriously damaged into line traces, and there is only a small portion of nanostructure chains occurring close to the groove edge. When the time delay becomes $\Delta t = 4$ ps, the serious damage of the groove surfaces almost disappeared, instead multiple spindle-like nanostructure chains began to emerge. Such kind of observation is further pronounced with larger time delays. With increasing the time delay to $\Delta t = 20$ ps, in spite of still formation of chains, we can find that the spatial distribution of the spindle-like nanostructure chains becomes degraded in both quality and quantity. Especially, when the time delay became as large as $\Delta t = 35$ ps, the nanostructure chains were seen difficult to form within the groove, which implies the time-delay dependent physical correlations between dual laser interaction processes.

Fig. 5 shows how the formation of spindle-like nanostructure chains inside the microgroove changes with the direction of the laser polarization at a given time delay of $\Delta t = 6$ ps. It is seen here that for both laser polarizations having different angles (θ) relative to the horizontal direction, the spatial orientation of the structure chains can be always kept parallel to the groove edges, but the spindle units are ready to have slantwise profiles. Another interesting point is that, with both laser polarizations deviating from the direction perpendicular to the groove

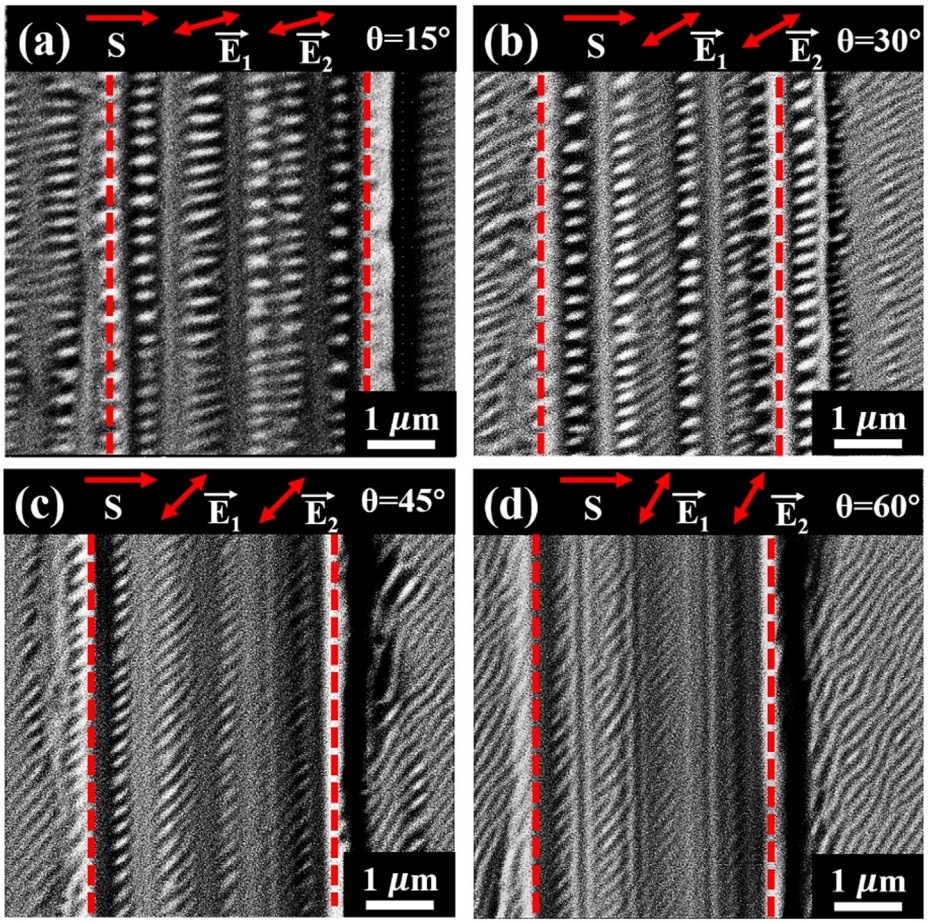

Fig. 5. Formation of spindle-like nanostructure chains inside the microgroove with changing the direction of both laser polarizations, which are represented by different θ angles relative to the horizontal direction. (a) θ = 15°; (b) θ = 30°; (c) θ = 45°; (d) θ = 60°.The total incident laser energy fluence is F = 42 mJ/cm^2 and the time delay of two laser beams is fixed at Δt = 6 ps.

edges, the formation of nanostructure chains inside the microgroove became decreased not only in number but also in geometric contrast. Especially, when the deviation angle increased to or larger than θ = 60°, the observation of nanostructure chains becomes rarely within the groove, indicating the physical role of the incident laser polarization.

Moreover, the influence of the laser energy fluence on the nanostructure chains formation was studied as well in the experiment. Based on a large quantity of experimental measurements, we successfully achieved the dependence of the spindle features (including the period, the major and minor length) on the laser fluence in a range of F = 30–50 mJ/cm^2, and the corresponding results are shown in Fig. 6. Here the employed other laser parameters are the same as Fig. 3, and each obtained value comes from averaging measurements of 20 spindle units. Clearly, with increasing the laser energy fluence, all structure parameters exhibit the enlarging variation tendencies. In specific, when the incident laser fluence was increased from F = 30 mJ/cm^2 to 50 mJ/cm^2, both major and minor lengths of the spindle units tend to are seen to gradually enlarge from 265 nm and 87 nm to the values of 449 nm and 191 nm, respectively; whereas its periodic configuration tends to improve from 163 nm to 293 nm. This phenomenon suggests an effective method to control the dimensions of spindle chains inside the microgroove.

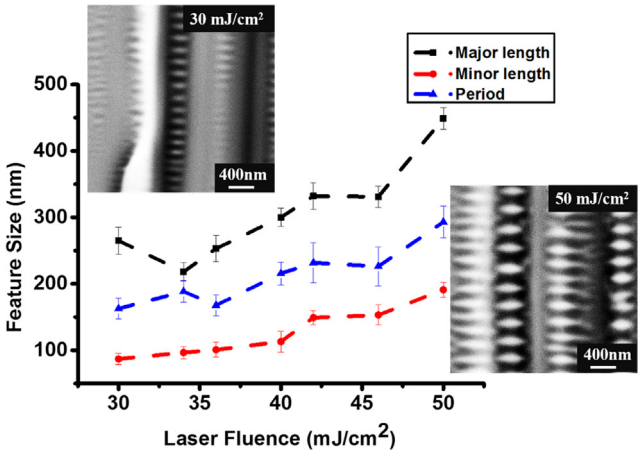

Fig. 6. Measured variations of the spindle feature dimension as a function of the incident laser fluence of two beams. Both upper-left and bottom-right insets show the SEM images of the nanostructure chains under the laser fluences of F = 30 mJ/cm^2 and 50 mJ/cm^2, respectively. The time delay of two laser beams is fixed at Δt = 6 ps and the sample scanning speed is v = 0.3 mm/s.

3.3. Formation of the single nanostructure chain in the submicron groove

During the aforementioned experiments, the opening width of the groove is several micrometers, about 5 times of the incident laser wavelength (800 nm), so that multiple chains of the spindle nanostructure can be formed. Now an open question is naturally raised: what happens for the narrower groove? By applying the same laser parameters in Fig. 3, we repeated the experiment on the submicron-scaled groove, and the corresponding results are shown in Fig. 7. It is clearly that there is only a single nanostructure chain formed within the groove, and structural units also display the spindle profile in geometry, very similar to the observations in the micro-scaled groove. In this case, the measured major and minor lengths of the spindle units are 410 nm and 130 nm, respectively, with the periodic spacing of about 200 nm. All these values are slightly larger than those in the microgroove. The

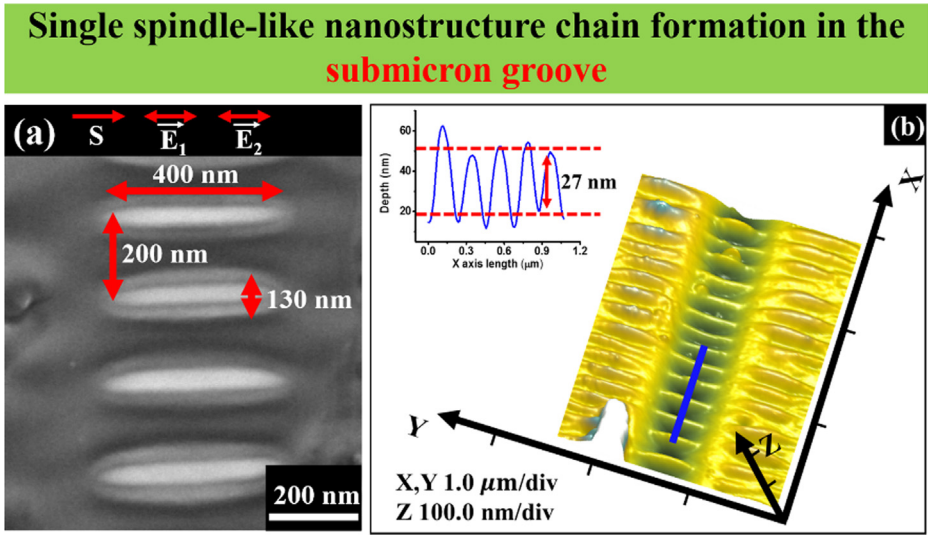

Fig. 7. Microscopic images of the single spindle chain formation within the submicron-scaled groove, with irradiation of two femtosecond laser beams at the time delay of $\Delta t = 6$ ps. (a) High-resolution SEM image of the nanostructure chain inside the groove. (b) Three-dimensional AFM image of the nanostructure formation inside and on the periphery of the groove. The upper-left inset shows the measured cross section profile of nanostructure chain formation (blue line) within the groove. (For interpretation of the references to colour in this figure legend, the reader is referred to the web version of this article.)

corresponding cross section curve of the AFM measurement reveals that the spindle structure height is about 27 nm. Moreover, it appears that the nanostructures distribution within the submicron groove becomes more regular and uniform. On the other hand, in contrast to the ordinary ripple structures formation on the flat surface near the scratched groove, the induced single chain of the spindle units seems to be well organized. Therefore, it is understood that the number of nanostructure chain formation can be controlled by the groove width.

3.4. Formation of random microstructures on the flat surface

During the above-mentioned experiments, the spindle-like nanostructures can be always found on the surface areas of both inside and closely outside the grooves. To explore the physical significance of the grooves for the regular formation of the spindle-like structures, we attempted to strike a flat sample surface with irradiation of two femtosecond laser beams, and the corresponding result is shown in Fig. 8, where the employed laser parameters are the same as Fig. 3 except for the totally incident energy fluence of $F = 50$ mJ/cm^2. In this case, the laser-induced surface structures are seen to mostly exhibit the ripple-like profiles, however, their spatial alignments are interrupted somewhere to cause the morphology of shallow spindle-like nanostructures,

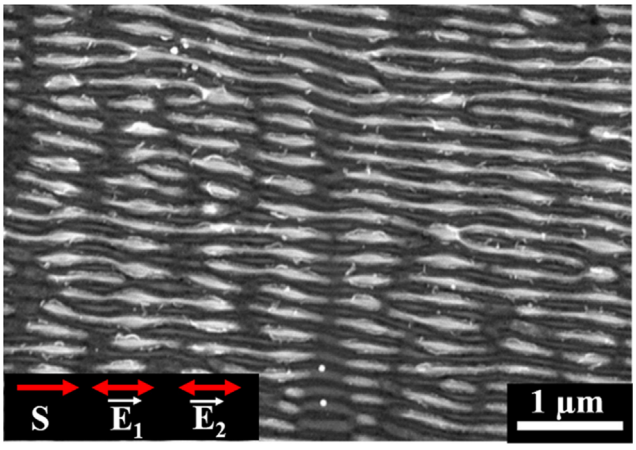

Fig. 8. Surface morphology of the nanostructures formed on the flat sample surface irradiated by two femtosecond laser beams at the time delay of $\Delta t = 6$ ps, where the total incident energy fluence is $F = 50$ mJ/cm^2 and the scanning speed is $v = 0.3$ mm/s. E_1 and E_2 represent directions of the laser polarizations, and S for the sample scanning direction.

in sharp contrast to the regular observations inside the microgroove. Accordingly, we can conclude that the geometric features of the micro/submicron-groove are essential to improve the quality and efficiency of the spindle-like nanostructure formation.

3.5. Exploration of the underlying mechanism

As for the good understanding of the experimental phenomena, the physical processes during the structure formation by femtosecond laser pulses should be explored in detail. First, for the micron-scaled groove, the achieved multiple spindle chains can be viewed as the spatial interlocking results between two types of laser-induced ripple structures: one is oriented always parallel to the groove edges (not being affected by the laser polarization), with the large period of about 667 nm in the spatial distribution; the other is oriented always parallel to the laser polarization, with the small period of about 200 nm in the spatial distribution. According to the previous studies [26–28], the former is originated from the intensity fringes of interference between the laser and the exited SPP that is coherently scattered from top edges of the groove. In other words, upon irradiation of femtosecond laser the top edges of the groove are ready to provoke the SPP excitation for the near enhanced electromagnetic field, which makes the spatial alignment of the intensity fringes along the groove edges [26]. Fig. 9 shows our simulation result using the FDTD method, and five intensity fringes of the enhanced SPP field can be evidenced within the groove.

Moreover, because the SPP excitation by the top edges of the groove would like to propagate in two opposite directions (left and right sides), the resultant intensity fringes parallel to the groove edges can be also found on the surface areas out of the groove, especially close to the top edges, as shown in Fig. 3a. It is known that the efficiency of SPP excitation by the top edges closely relies on the direction of the linear polarization of the incident femtosecond laser, and thus no plasmonic field scattering occurs when the laser polarization is parallel to the groove edges [29]. That is, the contrast of the intensity fringes formation reaches the maximum for the direction of the laser polarization perpendicular to the groove edges, while it is gradually degraded with changing the laser polarization direction. This is consistent with the experimental observations.

On the other hand, when the ferromagnetism of the sample material of Fe-based metallic glass is considered, the transverse electric (TE) mode of surface magnon polaritons (SMP) can be excited on the sidewall surfaces of the groove during the femtosecond laser irradiation [15], whose tangential wave vector, k_s, is written as

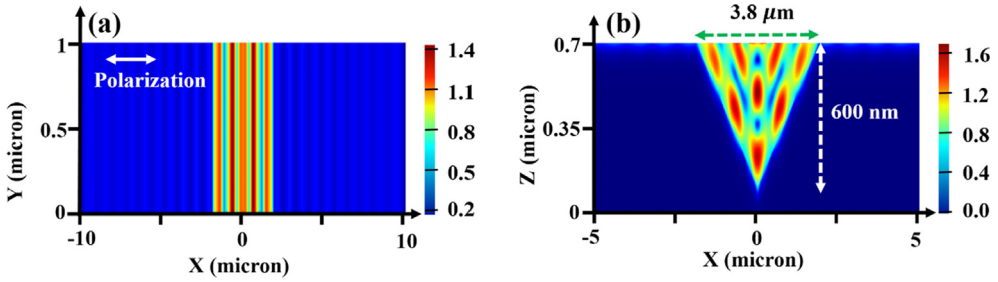

Fig. 9. Simulated optical field distribution patterns within the groove on Fe-based metallic glass surface, under irradiation of femtosecond laser with the linear polarization direction orthogonal to the groove edges. (a) X-Y plane; (b) X-Z plane.

$$k_S = \frac{\omega}{c}\sqrt{\left(\frac{\mu_2\varepsilon_1 - \mu_1\varepsilon_2}{\mu_2 - \mu_1}\right)\frac{\mu_1\mu_2}{\mu_1 + \mu_2}} \quad (1)$$

where ω is the angular frequency of the laser light, c for the light velocity, μ_i and ε_i (i = 1,2) for the real parts of the magnetic permeability and dielectric permittivity of the media, respectively. Similar to the ordinary ripple structure formation based on the SPP excitation, the optical interference between the femtosecond laser and the excited SMP consequently leads to the periodic structure formation on the groove surfaces, but with the spatial orientation parallel to the direction of the laser polarization. When the parameters of the surrounding air (i = 1) and the sample materials (i = 2) are assumed to be $\mu_1 = \varepsilon_1 = 1.00$, $\mu_2 = 1.20$, $\varepsilon_2 = -6.30$, we can obtain the spatial period of about 177 nm for the induced surface structures by the formula of $\Lambda_s = 2\pi/k_s$, which agrees with the experimental measurement of 180 nm.

Moreover, due to the orthogonal alignments, the intensity fringes induced by both SMP and SPP excitation tend to have spatial interlocking on the sidewalls of the groove, and the consequent ablation of the material surface brings about the multiple chains of the spindle nanostructures. For the submicron-scaled groove, the interval space between the top and bottom edges is significantly reduced, so that the SPP-based intensity fringes can no longer be included, *i.e.*, only SMP-based intensity fringes appear on two sidewall surfaces to show a single chain of the ablation nanostructures.

For the purpose of comparison, the irradiation of a single-beam femtosecond laser onto the grooves was also studied in the experiment, but it was often hard to see the chains of spindle nanostructure formation. According to the previous study, the larger electron–phonon coupling factor (g) of the material is beneficial for the femtosecond laser-induced periodic ripple structures [30]. Because the g factor of Fe-based metallic glass is relatively smaller in comparison with metals [31], almost no formation of the spindle nanostructures is caused. On the contrary, during the irradiation of two femtosecond laser beams the incident first laser beam is ready to promote the electron temperature of the material, which transiently improves the value of g factor [32–34], and thus the periodic structures induced by the second laser beam becomes more pronounced. Accordingly, when the time delay between two laser beams is sufficiently large, the transient increase of g factor from the first laser beam incidence tends to gradually vanish because of the decreasing electron temperature, which results in no appearance of the periodic structures within the groove.

4. Conclusion

In summary, we have employed two time-delayed femtosecond laser beams with the identical linear polarization, to successfully produce the regular chains of spindle nanostructures inside the microgrooves on the surface of Fe-based metallic glass. It has been found that the spatial alignment of spindle chains, with the period of about 667 nm, can always keep parallel to the groove edges even for different laser polarization directions. For the distribution of the spindle units, the measured spatial period is only about 180 nm, and their major and minor lengths approximate 350 nm and 120 nm, respectively. The contrast and the orientation of the spindle structures can be modulated by the incident laser polarization. The formation of the spindle chains disappeared for the laser polarization parallel to the groove edges. Moreover, when the groove width decreased to the submicron scale, only one chain of the spindle nanostructures was observed.

To give a satisfactory explanation of the observations, we have recognized such composite patterns as the spatial interlocking of two orthogonally oriented laser-induced structures: one is originated from the coherent SPP field generation by the groove edges, whose interference with the laser light consequently results in the subwavelength periodic intensity fringes parallel to the edges; the other from the excitation of TE-polarized SMP field on the sidewall surfaces due to the magnetic property of the material, whose interference with the laser light results in the deep-subwavelength periodic intensity fringes parallel to the laser polarization. Our investigations will not only benefit the understanding the physics of the laser-material interaction, but also be helpful in control developing nanostructures for the novel devices and applications, such as plasmonics [35], sensing [36] and catalysts [37].

CRediT authorship contribution statement

Zhen Zhao: Writing - original draft, Methodology, Software, Investigation, Writing - review & editing. **Bo Zhao:** Software, Writing - original draft, Writing - review & editing. **Yuhao Lei:** Writing - original draft. **Jianjun Yang:** Conceptualization, Writing - original draft, Writing - review & editing, Supervision, Project administration, Funding acquisition. **Chunlei Guo:** Project administration.

Declaration of Competing Interest

The authors declare that they have no known competing financial interests or personal relationships that could have appeared to influence the work reported in this paper.

Acknowledgements

This study was financially supported by National Natural Science Foundation of China (91750205, 11674178), K. C. Wong Education Foundation (GJTD-2018-08), Jilin Provincial Science & Technology Development Project (20180414019GH), Natural Science Foundation of Tianjin City (17JCZDJC37900), and Scientific and Technological Innovation Programs of Higher Education Institutions in Shanxi (2019L0902).

References

[1] D.K. Gramotnev, S.I. Bozhevolnyi, Plasmonics beyond the diffraction limit, Nat. Photonics 4 (2010) 83–91, https://doi.org/10.1038/nphoton.2009.282.
[2] W.L. Barnes, A. Dereux, T.W. Ebbesen, Surface plasmon subwavelength optics, Nature 424 (2003) 824–830, https://doi.org/10.1038/nature01937.
[3] J.K. Hwang, S. Cho, J.M. Dang, E.B. Kwak, K. Song, J. Moon, M.M. Sung, Direct

nanoprinting by liquid-bridge-mediated nanotransfer moulding, Nat. Nanotechnol. 5 (2010) 742–748, https://doi.org/10.1038/nnano.2010.175.
[4] S. Kim, B. Marelli, M.A. Brenckle, A.N. Mitropoulos, E. Gil, K. Tsioris, H. Tao, D.L. Kaplan, F.G. Omenetto, All-water-based electron-beam lithography using silk as a resist, Nat. Nanotechnol. 9 (2014) 306–310.
[5] V. Rinnerbauer, S. Ndao, Y.X. Yeng, J.J. Senkevich, K.F. Jensen, J.D. Joannopoulos, Large-area fabrication of high aspect ratio tantalum photonic crystals for high temperature selective emitters, J. Vac. Sci. Technol. B 31 (2013) 011802, , https://doi.org/10.1116/1.4771901.
[6] H. Qiao, J. Yang, F. Wang, Y. Yang, J. Sun, Femtosecond laser direct writing of large-area two-dimensional metallic photonic crystal structures on tungsten surfaces, Opt. Express 23 (2015) 26617–26627, https://doi.org/10.1364/OE.23.026617.
[7] K. Sugioka, Y. Cheng, Ultrafast lasers-reliable tools for advanced materials processing, Light-Sci. Appl. 3 (2014) e149, , https://doi.org/10.1038/lsa.2014.30.
[8] G. Deng, G. Feng, S. Zhou, Experimental and FDTD study of silicon surface morphology induced by femtosecond laser irradiation at a high substrate temperature, Opt. Express 7 (2017) 7818–7827, https://doi.org/10.1364/OE.25.007818.
[9] S. Baudach, J. Bonse, W. Kautek, Ablation experiments on polyimide with femtosecond laser pulses, Appl. Phys. A 69 (1999) S395–S398.
[10] A.Y. Vorobyev, C. Guo, Antireflection effect of femtosecond laser-induced periodic surface structures on silicon, Opt. Express 19 (2011) A1031–A1036, https://doi.org/10.1364/OE.19.0A1031.
[11] Z. Ou, M. Huang, F. Zhao, Colorizing pure copper surface by ultrafast laser-induced near-subwavelength ripples, Opt. Express 22 (2014) 17254–17265, https://doi.org/10.1364/OE.22.017254.
[12] M. Huang, F. Zhao, Y. Cheng, N. Xu, Z. Xu, Origin of laser-induced near-subwavelength ripples: interference between surface plasmons and incident laser, ACS Nano 3 (2009) 4062–4070, https://doi.org/10.1021/nn900654v.
[13] Y. Shimotsuma, P.G. Kazansky, J. Qiu, K. Hirao, Self-organized nanogratings in glass irradiated by ultrashort light pulses, Phys. Rev. Lett. 91 (2003) 247405, , https://doi.org/10.1103/PhysRevLett.91.247405.
[14] V. Khuat, J. Si, T. Chen, X. Hou, Deep-subwavelength nanohole arrays embedded in nanoripples fabricated by femtosecond laser irradiation, Opt. Lett. 40 (2015) 209–212, https://doi.org/10.1364/OL.40.000209.
[15] C.H.R. Ooi, K.C. Low, R. Higa, T. Ogawa, Surface polaritons with arbitrary magnetic and dielectric materials: new regimes, effects of negative index, and superconductors, J. Opt. Soc. Am. B 29 (2012) 2691–2697, https://doi.org/10.1364/JOSAB.29.002691.
[16] V.H. Arakelian, L.A. Bagdassarian, S.G. Simonian, Electrodynamics of bulk and surface normal magnon-polaritons in antiferromagnetic crystals, J. Magn. Magn. Mater. 167 (1997) 149–160, https://doi.org/10.1016/S0304-8853(96)00299-5.
[17] Z. Sun, X. Zuo, T. Guan, W. Chen, Artificial TE-mode surface waves at metal surfaces mimicking surface plasmons, Opt. Express 22 (2014) 4714–4722, https://doi.org/10.1364/OE.22.004714.
[18] A. Hartstein, E. Burstein, A.A. Maradudin, R. Brewer, R.F. Wallis, Surface polaritons on semi-infinite gyromagnetic media, J. Phys. C Solid Stat Phys. 6 (1973) 1266–1276, https://doi.org/10.1088/0022-3719/6/7/016.
[19] Y. Yuan, Y. Lin, B. Gu, N. Panwar, S.C. Tjin, J. Song, J. Qu, K. Yong, Optical trapping-assisted SERS platform for chemical and biosensing applications: Design perspectives, Coord. Chem. Rev. 339 (2017) 138–152, https://doi.org/10.1016/j.ccr.2017.03.013.
[20] E.D. Diebold, N.H. Mack, S.K. Doorn, E. Mazur, Femtosecond laser-nanostructured substrates for surface-enhanced Raman scattering, Langmuir 25 (2009) 1790–1794, https://pubs.acs.org/doi/full/10.1021/la803357q.
[21] S.A. Maier, P.G. Kik, H.A. Atwater, S. Meltzer, E. Harel, B.E. Koel, A. Requicha, Local detection of electromagnetic energy transport below the diffraction limit in metal nanoparticle plasmon waveguides, Nat. Mater. 2 (2003) 229–232, https://doi.org/10.1038/nmat852.
[22] G. Dumitru, V. Romano, H.P. Weber, M. Sentis, W. Marine, Femtosecond ablation of ultrahard materials, Appl. Phys. A 74 (2002) 729–739.
[23] J. Wang, Y. Liu, M. Chen, G. Xie, D.V. Louzguine-Luzgin, A. Inoue, J.H. Perepezko, Rapid degradation of azo dye by Fe-based metallic glass powder, Adv. Funct. Mater. 22 (2012) 2567–2570, https://doi.org/10.1002/adfm.201103015.
[24] A. Inoue, A. Takeuchi, Recent development and application products of bulk glassy alloys, Acta Mater. 59 (2011) 2243–2266, https://doi.org/10.1016/j.actamat.2010.11.027.
[25] N. Saegusa, A. H. Morrish, Mössbauer study of amorphous Fe81B13.5Si3.5C2, Phys. Rev. B 26 (1982) 10-15, https://doi.org/10.1103/physrevb.26.10.
[26] O. Go, M. Naoki, M. Tomoya, T. Mitsuhiro, N.N. Nedyalkov, O. Minoru, Plasmonic and mie scattering control of far-field interference for regular ripple formation on various material substrates, Opt. Express 19 (2011) 19093–19103, https://doi.org/10.1364/OE.19.019093.
[27] R.D. Murphy, B. Torralva, D.P. Adams, S.M. Yalisove, Polarization dependent formation of femtosecond laser-induced periodic surface structures near stepped features, Appl. Phys. Lett. 104 (2014) 231117, , https://doi.org/10.1063/1.4882998.
[28] K. Miyazaki, G. Miyaji, T. Inoue, Nanograting formation on metals in air with interfering femtosecond laser pulses, Appl. Phys. Lett. 107 (2015) 071103, , https://doi.org/10.1063/1.4928670.
[29] C. Li, G. Cheng, J. P. Colombier, N. Faure, S. Reynaud, H. Zhang, D. Jamon, R. Stoian, Impact of evolving surface nanoscale topologies in femtosecond laser structuring of Ni-based superalloy CMSX-4, J. Opt. 18 (2016) 015402, http://iopscience.iop.org/2040-8986/18/1/015402.
[30] J. Wang, C. Guo, Ultrafast dynamics of femtosecond laser-induced periodic surface pattern formation on metals, Appl. Phys. Lett. 87 (2005) 251914, , https://doi.org/10.1063/1.2146067.
[31] S. Marinier, L.J. Lewis, Femtosecond laser ablation of Cu_xZr_{1-x} bulk metallic glasses: a molecular dynamics study, Phys. Rev. B 92 (2015) 184108, , https://doi.org/10.1103/PhysRevB.92.184108.
[32] G. Du, Q. Yang, F. Chen, Y. Wu, Y. Ou, Y. Lu, X. Hou, Ultrafast thermalization dynamics in two-layer metal films excited by temporally shaped femtosecond laser, Int. J. Heat Mass Transf. 87 (2015) 341–346, https://doi.org/10.1016/j.ijheatmasstransfer.2015.03.090.
[33] G. Du, Y. Wu, N. Uddin, Q. Yang, F. Chen, Y. Lu, H. Bian, X. Hou, Ultrafast thermal dynamics of nano-ripples formation via laser double pulses excitation, Opt. Commun. 375 (2016) 54–57, https://doi.org/10.1016/j.optcom.2016.04.064.
[34] G. Du, F. Chen, Q. Yang, J. Si, X. Hou, Ultrafast thermalization characteristics in Au film irradiated by temporally shaped femtosecond laser pulses, Opt. Commun. 284 (2011) 640–645, https://doi.org/10.1016/j.optcom.2010.09.061.
[35] S.A. Maier, M.L. Brongersma, P.G. Kik, S. Meltzer, A.G. Requicha, H.A. Atwater, Plasmonics – a route to nanoscale optical devices, Adv. Mater. 13 (2001) 1501–1505, https://doi.org/10.1002/1521-4095(200110)13:19 < 1501::AID-ADMA1501 > 3.0.CO;2-Z.
[36] A.I. Kuznetsov, A.B. Evlyukhin, M.R. Goncalves, C. Reinhardt, A. Koroleva, M.L. Arnedillo, R. Kiyan, O. Marti, B.N. Chichkov, Laser fabrication of large-scale nanoparticle arrays for sensing applications, ACS Nano 5 (2011) 4843–4849, https://doi.org/10.1021/nn2009112.
[37] U. Sahaym, M.G. Norton, Advances in the application of nanotechnology in enabling a 'hydrogen economy', J. Mater. Sci. 43 (2008) 5395–5429.